Temperature dependence of fluorescence spectra from x-ray-excited single-crystal CaF_2:Mn(x) (x=0.1, 1.0, 3.0 at. %)

Joanne F. Rhodes, R. J. Abbundi, D. Wayne Cooke,* V. K. Mathur, and M. D. Brown
Naval Surface Weapons Center, White Oak, Silver Spring, Maryland 20910
(Received 16 November 1984)

Fluorescence spectra of x-ray-excited single-crystal CaF_2:Mn were methodically measured with a silicon-diode array at intervals over the temperature range of 13—670 K for samples with 0.1-, 1.0-, and 3.0-at. % Mn concentration. All spectra exhibited a non-Gaussian broadband emission skewed to the high-wavelength side and centered near 500 nm. The full width at half maximum increased with temperature from approximately 0.18 to 0.31 eV, with slight variation between the three samples. A fit of these data to the well-known expression for the full width of an emission band as a function of temperature, $W(T)=W(0)[\coth(\hbar\omega/2k_BT)]^{1/2}$, yielded values of approximately 0.20 eV for $W(0)$, and 7.4×10^{13} sec^{-1} for the excited-state vibrational frequency ω. However, this functional form does not adequately describe these data over an extended temperature range. The centroid of the distribution for all concentrations shifted 3.9—6.4 nm toward shorter wavelengths as the temperature increased from 13 to 375 K, then shifted 0.9—2.1 nm toward longer wavelengths as the temperature rose to 670 K. From 13 to approximately 325 K, the area of the spectral distribution increased by a factor of 2—4. With further temperature increase the area quenched to less than 5% of its maximum value. From the data for each concentration an activation energy for thermal quenching was extracted. These values were found to be 1.27, 0.91, and 0.91 eV for samples with 0.1-, 1.0-, and 3.0-at. % Mn concentration. Spectral analyses showed that a decrease of Mn concentration was accompanied by an increase in skewness and a decrease in centroid wavelength.

I. INTRODUCTION

CaF_2 doped with manganese (Mn) has long been a subject of considerable interest. Much of this interest has centered around its important application as a thermoluminescent radiation dosimeter.[1] This is a result of the wide-range linearity of its thermoluminescent response to radiation dose, its high sensitivity to low dose, and the location of a major glow peak well above room temperature.

Investigations of its optical properties[2—13] have received particular attention. It has been reported[8] that the emission spectrum of x-irradiated CaF_2:Mn contains a weak emission peak at 280 nm which has been attributed to radiative recombination of electrons with holes, and a major peak near 500 nm. Although the 500-nm emission has been attributed[8,9] to the deexcitation of Mn^{2+}, investigators[2,4,8] have suggested a variety of processes for the formation mechanism of the excited Mn^{2+} ion. Most of these processes are primarily associated with a particular CaF_2:Mn glow peak. The glow curve for CaF_2:Mn(0.1 at. %) using a 0.1-K/sec heating rate is shown in Fig. 1. Three peaks of interest are located approximately at 100, 200, and 520 K. The exact temperature at which a glow peak occurs depends on the employed heating rate. Theoretical and experimental investigations have indicated that the 100-K peak is due to V_K centers,[4] while the 200-K peak has been attributed[8] to V_{KA} centers. It has been suggested[8,10] that Mn^+ is formed under low-temperature x irradiation, with simultaneous trapping of a hole at a lattice site, and that Mn^+ is converted to Mn^{2+} when heated to 200 K.[8] This charge conversion is attributed to the detrapping of the holes responsible for the glow peaks at 100 and 200 K. Although the nature of the trap has not been specified, the 520-K dosimetry peak has been attributed to electron trapping.[2]

We have performed a systematic study of CaF_2:Mn emission spectra over a wide temperature range covering all the major glow peaks. In addition to the advantages of

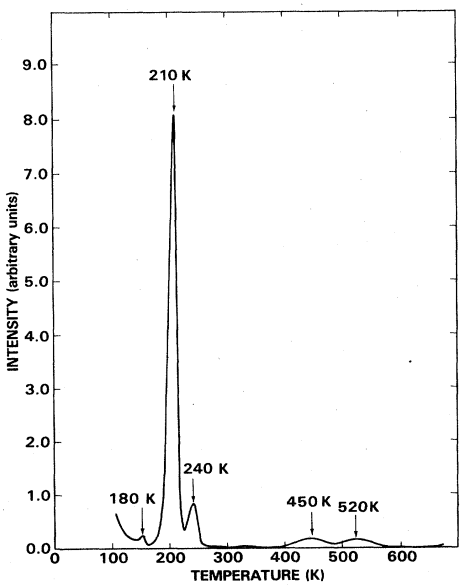

FIG. 1. Thermoluminescence glow curve for CaF_2:Mn(0.1 at. %) with a heating rate of 0.1 K/sec.

a repeatable spectrum-collection procedure, the use of a silicon-diode-array detector allowed the collection of many more spectra with higher spectral resolution than would have been feasible with the use of standard technology. Temperature-dependence studies were performed for three concentrations of Mn dopant to investigate the effect of Mn concentration on the emission. Analyses of each collected set of spectra provided a graphic description of the temperature dependence of the spectral area, centroid, skewness, and full width at half maximum (FWHM). These systematic studies have revealed subtle, previously unreported variations in the spectral behavior. Explanations are suggested for some of the salient features found in the analyses.

II. EXPERIMENTAL SETUP AND PROCEDURE

A diagram of the experimental setup is shown in Fig. 2. A 10-mm-diam, 2-mm-thick CaF_2:Mn single crystal of (100) orientation, obtained from Optovac, Inc., was affixed to a copper block and mounted in a chamber evacuated to a pressure of $\sim 10^{-6}$ Torr. The crystal faced in a direction 45° from both the x-ray source and the spectrograph entrance slit. The rhodium-target x-ray tube was operated at 30 kV and 0.29 mA to provide a dose rate of ~ 50 rad/min at the crystal position 9 cm away. A beryllium window was installed on the x-ray side of the sample chamber in order to pass x rays but block room light while maintaining a vacuum. The spectrograph viewed the crystal through a quartz lens mounted in the sample chamber.

The spectrograph employed a 100-μm entrance slit, and a 300-nm blazed, 300-groove/mm grating with a spectral range of 200—800 nm. The image from the spectrograph was focused onto a silicon-diode array of 1024 elements with a resulting resolution of 0.293 nm/channel. The spectral region viewed was chosen to be between 330 and 630 nm to cover the major emission band. This array was controlled by a microcomputer-based rapid-scanning spectrometer, which was part of a Tracor Northern multichannel-analyzer system used in data manipulations and analyses. The diode array allows simultaneous acquisition of the entire fluorescence spectrum within the region of interest. This data-accumulation process is much faster than a standard monochromator—photomultiplier-tube system, and thus requires less irradiation for adequate detection.

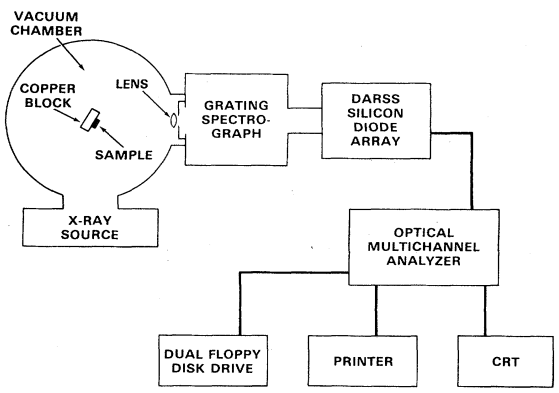

FIG. 2. Schematic diagram of the experimental setup.

The data were accumulated, beginning at low temperature, using the following procedure. The temperature of the sample was stabilized to within ± 0.1 K, and a background spectrum was recorded. Immediately following this, the fluorescence spectrum was recorded under identical conditions. After a background subtraction was performed, the resulting spectrum was smoothed using a three-point summing algorithm and stored. An identical procedure was repeated at each temperature.

Mn^{2+} is centrosymmetric in CaF_2, and this symmetry results in an isotropic crystal structure. The emission from CaF_2:Mn is therefore expected to be unpolarized, and we have experimentally found this to be true. Moreover, the polarizing effect caused by the spectrograph grating[14] was found to be negligible, and was therefore not taken into account in subsequent analyses.

Each spectrum was corrected for system-efficiency variations in wavelength with the use of a 45-W tungsten-halogen lamp as a reference. Additionally, the data were normalized at room temperature to account for the measured intensity difference inherent in the low- and high-temperature setups.

III. EXPERIMENTAL RESULTS AND ANALYSES

All observed fluorescence spectra of CaF_2:Mn exhibited a non-Gaussian broadband distribution skewed to the high-wavelength side and centered near 500 nm. Some representative spectra are shown in Fig. 3. The full width at half maximum, centroid, skewness, and area were calculated for each spectral distribution. The temperature

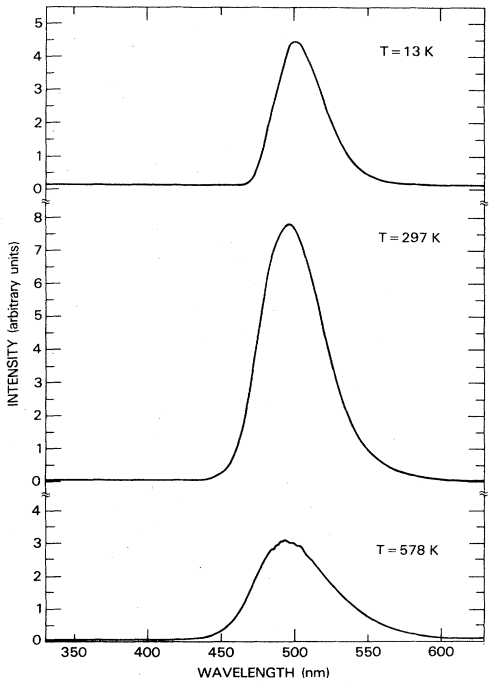

FIG. 3. Representative spectra of CaF_2:Mn(3.0 at. %) at different temperatures.

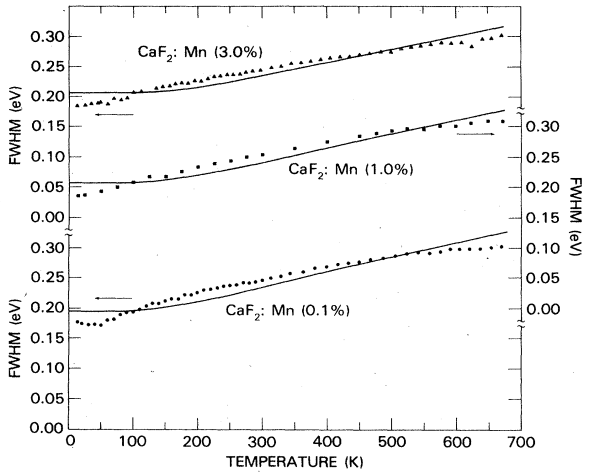

FIG. 4. Spectral full width at half maximum temperature evolution and theoretical fits for three Mn concentrations.

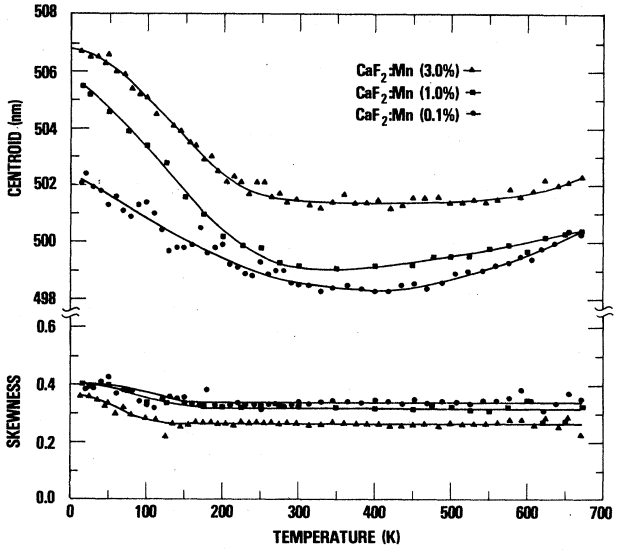

FIG. 5. Spectral centroid and skewness temperature evolutions for three Mn concentrations.

variation of these quantities, as well as some additional analyses, are presented below.

The spectral FWHM for each sample increased fairly smoothly with temperature, as shown in Fig. 4. The FWHM ranged from low-temperature values of 0.19, 0.19, and 0.18 eV, to high-temperature values of 0.30, 0.31, and 0.30 eV for 3.0-, 1.0-, and 0.1-at. % Mn concentrations, respectively.

The solid curves in the figure represent the least-squares fits of the experimental results to the well-known theoretical expression[15–17] for the full width of an emission band, namely,

$$W(T)=W(0)[\coth(\hbar\omega/2k_BT)]^{1/2}\,, \tag{1}$$

where $W(T)$ is the FWHM at temperature T, $W(0)$ is the FWHM extrapolated to 0 K, and $\hbar\omega$ is the vibrational quantum of the ion in the excited state. The extracted parameters, $W(0)$, ω, and the average percent error for each fit, are given in Table I. The quality of fit is approximately the same for each Mn concentration, and the ω value increases only slightly as Mn concentration increases.

The temperature variation of the centroid for each Mn concentration is shown in Fig. 5. As temperature increased from 13 to 375 K, the centroid shifted 5.3, 6.4, and 3.9 nm toward lower wavelength for the 3.0-, 1.0-, and 0.1-at. % Mn samples, respectively. Further temperature increase met with 0.9-, 1.3-, and 2.1-nm shifts back toward higher wavelength for the same respective samples. As shown in the figure, a decreased Mn concentration was accompanied by a small but detectable decrease in centroid wavelength.

Also shown in Fig. 5 is the dependence of skewness on temperature for the three Mn concentrations. It can be seen here that skewness is independent of temperature, except at very low temperatures. The skewness decreases as Mn concentration increases from 1.0 to 3.0 at. %. However, it is difficult to clearly separate the 0.1- and 1.0-at. % Mn data. The skewness is calculated as the third central moment of the spectral distribution, and its magnitude is thus more sensitive to variations in the spectral wings than is the centroid. The limits of the spectral window were chosen to be at the 10% peak-intensity points in order to avoid contributions from baseline noise.

TABLE I. Extracted parameters and percent error for a functional fit of full width at half maximum for samples with three Mn concentrations.

Mn conc. (at. %)	$W(0)$ (eV)	ω ($\sec^{-1}$) ($\times 10^{13}$)	Average error (%)
3.0	0.208	8.13	4.1
1.0	0.208	7.51	4.3
0.1	0.196	6.68	5.0
Avg.	0.204	7.44	4.5

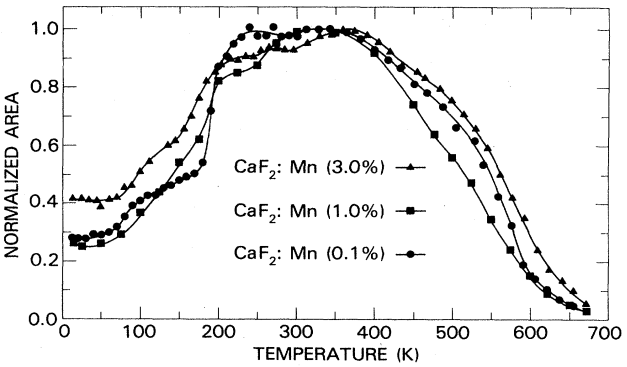

FIG. 6. Integrated spectral intensity temperature evolution for three Mn concentrations.

TABLE II. Parameters extracted from a three-parameter fit for the N highest-temperature points of the quenching data.

Mn conc. (at. %)	N	E (eV)	s/p_r	I_0	p_n/p_r 550 K	p_n/p_r 600 K
3.0	9	0.91	6.69×10^{7}	0.73	0.32	1.56
1.0	6	0.91	1.21×10^{8}	0.56	0.57	2.82
0.1	5	1.27	2.86×10^{10}	0.25	0.07	0.64

The final spectral characteristic discussed here is the integrated intensity (area) of the emission band. Figure 6 shows the response of this intensity to temperature for each concentration of Mn. Each curve is normalized to unity at its maximum value.

Several characteristics may be observed from these curves. All three samples have sharp intensity increases in the (150—250)-K temperature range. The 3.0- and 0.1-at. % Mn samples have a small knee between ~75 and 150 K, while the 1.0-at. % Mn sample has a knee between ~180 and 250 K. Interestingly, the rate of area change near 200 K is noticeably larger for the 0.1-at. % Mn sample than for the other two.

Not indicated in the figure is the fact that the measured room-temperature intensity produced by the 3.0-at.% Mn sample was approximately the same as that of the 1.0-at. % Mn sample, and was a factor of 2 larger than that of the 0.1-at. % Mn sample. However, relative intensity could not be specified with great accuracy because of the sensitivity of the setup to crystal position.

The high-temperature portions of the area curves were fit to a theoretical function[18] which predicts thermal quenching. This function is given as

$$I(T)=I_0[1+(s/p_r)\exp(-E/k_BT)]^{-1}, \quad (2)$$

where $I(T)$ is the intensity at temperature T, I_0 is the intensity prior to commencement of the high-temperature quenching, s is a preexponential factor, p_r is the probability of radiative transitions, and E is the energy of activation for thermal quenching.

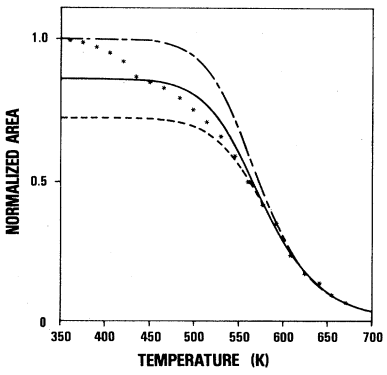

FIG. 7. Temperature-quenching portion of integrated intensity curve for CaF_2:Mn(3.0 at. %) and three theoretical fits: Solid line, three-parameter fit of data; long-dashed—short-dashed line, one-parameter fit of data; dashed line, three-parameter fit of nine highest-temperature data points.

A variety of fits was done because the data were not described well by Eq. (2). Shown in Fig. 7 are the graphs of the high-temperature area curve for the 3.0-at. % Mn sample, a three-parameter fit and a one-parameter fit of the quenching data set, and a three-parameter fit of the nine highest-temperature data points to Eq. (2). In the high-temperature region of the curve, the exponential term of the equation is dominant. Since a three-parameter fit with less than 6.0% error could be obtained from the highest-temperature points, a value of E was extracted from this type of fit with some confidence. A one-parameter fit was done for all of the quenching data in order to most effectively demonstrate the differences between the shape of the theoretical function and the shape of the experimental data. This was done by setting E equal to the value extracted from the previously described fit, setting I_0 equal to the maximum area value, and then extracting a value for s/p_r. The E, I_0, and s/p_r values from the three-parameter fit of the N highest-temperature data points for each Mn concentration are shown in Table II. The data set was normalized to unity at the maximum.

After completion of the experiment, neutron-activation and x-ray-fluorescence analyses were performed on the three samples to determine their trace-element composition. The results revealed that the Optovac crystals formed from preparates of 3.0-, 1.0-, and 0.1-at. % Mn concentration were actually of 1.43-, 0.70-, and 0.11-at. % Mn concentration, respectively. Table III lists trace-element concentrations of the most prominent constituents.

TABLE III. Concentrations of important elements obtained by neutron-activation analysis (ppm unless specified).

Element	Mn concentration (at. %) 0.1	1.0	3.0
Na	96±5	91±5	90±5
Fe	80±30	60±30	60±30
Sr	240±20	240±10	140±20
Ba	55±13	250±20	420±30
La	15.4±0.8	18.5±0.9	14.5±0.7
Ce	0.75±0.22	0.10±0.03	0.54±0.26
Sm[a]	1.48±9	108±6	105±8
Yb	0.18±0.06	0.13±0.04	0.18±0.06

[a]ppb.

IV. DISCUSSION

Although the behavior of the full width at half maximum is approximately in accordance with Eq. (1), examination of the experimental data reveals that its shape is slightly concave downward rather than as described by the equation. The data points are causally distributed rather than randomly scattered on both sides of the function. This shows that, although the average percent error is reasonable in each fit, Eq. (1) is not completely descriptive of the processes involved.

In addition to the experimental evidence above, there are also some theoretical reasons to question the degree of applicability of Eq. (1) to the data. The theory[15–17] from which Eq. (1) is derived predicts a Gaussian spectral distribution and a temperature-independent spectral band centroid. However, as indicated earlier, these spectra are skewed, and the centroid does have a temperature dependence. The possibility that these factors are partially responsible for the observed difference between theory and experiment must at least be considered.

The behavior of the centroid as a function of temperature is significant, and has not been previously reported. It may be partially explained by thermal expansion of the crystal lattice. This can be seen with an examination of the Tanabe-Sugano diagram for Mn^{2+} in O_h symmetry. The emission found in CaF_2:Mn has been attributed[9] to the transition from the first-excited level $^4T_{1g}(^4G)$ to the ground state $^6A_{1g}(^6S)$. Recall that as temperature increases to 375 K, the centroid wavelength decreases for all three samples investigated. It is well known that a temperature increase reduces the crystal-field strength by increasing the average distance between the emitting center and its nearest neighbors. From the Tanabe-Sugano diagram it can be seen that a reduction of Dq is accompanied by higher-energy transitions. Thus, a shift of the centroid to lower wavelength results. However, preliminary calculations show that the centroid shift arising from thermal expansion is too small to explain our experimental results, and produces an incorrect functional form for the temperature dependence observed. In addition, this explanation does not account for the observed upturn in the centroid above 375 K, and, in fact, predicts opposite behavior.

Another possible explanation for the centroid shift is the formation of Mn^+ with low-temperature irradiation. Most importantly, there is evidence[8] that it is thermally annealed near 200 K. It is possible that environmental changes due to the decrease in Mn^+ concentration could affect the crystal field "seen" by Mn^{2+} in such a way as to cause the observed temperature dependence. The exact mechanism of this cause, however, remains unclear.

The occurrence of the relatively sharp increases in area which appear in the (100—200)-K data for all three samples is significant. The intensity curve of CaF_2:Mn was previously found[19] to exhibit a change in slope in the temperature range of a major glow peak. This prior work contained a theoretical study of the effect of traps on fluorescence yield, and used trap-filling theory[20] as a basis for investigation.

The degree to which fluorescence measurements are affected by traps depends on the temperature of the sample relative to the temperature of the glow peak. At temperatures far below the glow-peak temperature, a fraction of the free carriers generated by incident radiation are captured by the traps and are therefore not available for radiative recombination. At a temperature near that of the glow peak, or above it, traps are unable to hold carriers due to the high probability of thermal activation. Consequently, all the available free carriers may radiatively recombine and thus enhance the fluorescence yield. As the temperature is increased from the former case to the latter, a sharp increase in fluorescence yield is expected due to the increase in detrapping probability.

Examination of the glow peaks shown in Fig. 1 verifies that there is an intense glow peak in the temperature region where the integrated intensity has the greatest increase, namely around 200 K. The experimental evidence is thus consistent with the theory described above. It may be noted that the 0.1-at. % Mn curve exhibits a much sharper rise near 200 K and a slightly sharper decrease near 520 K than do the other two curves. Increased clustering effects in the more heavily doped samples make the 0.1-at. % Mn results more indicative of the ongoing physical processes for isolated Mn ions.

In summarizing possible related phenomena, it should be pointed out that the 210-K thermoluminescence (TL) peak occurs at the same temperature at which Mn^+ is thought to be rapidly charge-converted[8] to Mn^{2+}. Thus, the Mn^+ concentration, the centroid curve, the intensity curve, and the TL curve all exhibit a significant change at approximately the same temperature. Some type of hole center would be needed to charge-compensate for the presence of Mn^+, and could be responsible for the 210 glow peak.

The configuration-coordinate model has been shown[16] to yield the relatively small value of 3.35×10^{-10} cm for the displacement between the minima of excited- and ground-state potential-energy curves for divalent Mn in zinc silicate. The long-wavelength tail observed in the skewed emission spectrum was attributed to this small separation. The skewed emission in our work may be similarly explained. It was also noted that the small displacement value could imply the existence of a weak coupling between the Mn and the lattice.

As mentioned earlier, a concentration dependence exists for several parameters. The data show that, as Mn concentration decreases, the spectral skewness increases, the centroid shifts to smaller wavelength, and the extracted vibrational frequency ω decreases. Unfortunately, no explanation has been found which directly links change of Mn concentration with any of the observed behavior, except the shift of the centroid. It may be that an increase in the Mn concentration causes a change in the environment which results in an increase in the crystal-field parameter Dq. An increase in Dq results in lower-energy transitions and, thus, longer-wavelength emission.

The ratios of probabilities of nonradiative (p_n) to radiative (p_r) transitions were calculated for temperatures of 550 and 600 K from the parameters listed in Table II, and are shown there. It was observed that the ratios for larger Mn concentrations (3.0 and 1.0 at. %) were larger than the

ratios for the smaller Mn concentration (0.1 at. %). This suggests that cluster formation at higher Mn concentrations increases thermal quenching.

The possibility that the 500-nm emission band is actually composed of two closely spaced emission peaks was considered. These two emissions could arise from Mn^{2+} ions in two slightly different types of lattice sites. The change of Mn^{+} concentration near 200 K may be one of the factors which change the environment. Under these conditions, the shift of the centroid could then be explained by the growth of one emission at the expense of the other. However, no conclusive experimental evidence in support of this possibility has been obtained.

V. SUMMARY AND CONCLUSION

Analyses of CaF_2:Mn fluorescence spectra indicate that centroid position and spectral skewness depend on Mn concentration. Changes in these quantities resulting from concentration change are detectable, but are not major.

There is evidence that established theory predicts the temperature dependence of the full width at half maximum in a general manner, but must be refined to effectively describe the detailed behavior. In its present form this theory does not allow for a skewness of the emission or a temperature dependence of the centroid. The observed centroid behavior is thought to be caused by changes in the local crystal field "seen" by the Mn^{2+} ion.

Changes in the slopes of the area-versus-temperature curves are found in the temperature ranges of thermoluminescence glow peaks, and could be caused by the presence of traps. The most compelling evidence is the presence of the 200-K glow peak attributed to trapped holes with simultaneous formation of Mn^{+}. It is suggested that the shape of glow peaks in the temperature region of thermal quenching should be corrected for the effects of the quenching before kinetic analyses are attempted.

ACKNOWLEDGMENTS

The authors acknowledge S. W. S. McKeever and J. R. Cullen for helpful discussions, and Hei W. Chan for experimental assistance. David L. Anderson is acknowledged for the performance of neutron-activation analyses. This work was supported in part by the Naval Surface Weapons Center Independent Research Fund.

*Present address: Los Alamos National Laboratory, Los Alamos, NM 87545.

[1]James H. Schulman, Frank H. Attix, Edward J. West, and Robert J. Ginther, Rev. Sci. Instrum. **31**, 1263 (1960).

[2]James H. Schulman, in *Proceedings of the Symposium on Solid State and Chemical Radiation Dosimetry in Medicine and Biology* (IAEA, Vienna, 1967), p. 3.

[3]M. D. Agrawal and K. V. Rao, Phys. Status Solidi A **3**, 153 (1970).

[4]J. H. Beaumont, W. Hayes, D. L. Kirk, and G. P. Summers, Proc. R. Soc. London, Ser. A **315**, 69 (1970).

[5]M. D. Agrawal and K. V. Rao, Phys. Status Solidi A **6**, 693 (1971).

[6]M. D. Agrawal and K. V. Rao, Phys. Status Solidi A **14**, 217 (1972).

[7]P. J. Alonso, V. M. Orera, and R. Alcala, Phys. Status Solidi B **99**, 585 (1980).

[8]R. Alcala, P. J. Alonso, G. Lalinde, and A. Carretero, Phys. Status Solidi B **98**, 315 (1980).

[9]P. J. Alonso and R. Alcala, J. Lumin. **22**, 321 (1980).

[10]P. G. Baranov, Fiz. Tverd. Tela (Leningrad) **22**, 229 (1980) [Sov. Phys.—Solid State **22**, 133 (1980)].

[11]D. Wayne Cooke, Evangelos P. Gavathas, and M. D. Brown, J. Appl. Phys. **54**, 1165 (1983).

[12]C. M. Sunta, Radiat. Prot. Dosim. **8**, 25 (1984).

[13]R. J. Abbundi, D. W. Cooke, V. K. Mathur, G. A. Royce, and M. D. Brown, Radiat. Prot. Dosim. **6**, 329 (1984).

[14]T. D. S. Hamilton, I. H. Munro, and G. Walker, in *Luminescence Spectroscopy,* edited by Michael D. Lumb (Academic, New York, 1978), p. 191.

[15]Baldassare DiBartolo, *Optical Interactions in Solids* (Wiley, New York, 1968), pp. 420—426.

[16]Clifford C. Klick and James H. Schulman, J. Opt. Soc. Am. **42**, 910 (1952).

[17]D. Curie, *Luminescence in Crystals* (Wiley, New York, 1963), pp. 44—55.

[18]Clifford C. Klick and James H. Schulman, in *Solid State Physics,* edited by F. Seitz and D. Turnbull (Academic, New York, 1957), Vol. 5, pp. 99—102.

[19]S. G. Gorbics, A. E. Nash, and F. H. Attix, Int. J. Appl. Radiat. Isotopes **20**, 829 (1969).

[20]J. T. Randall and M. H. F. Wilkins, Proc. R. Soc. London, Ser. A **184**, 366 (1945).